 CMES, vol.3, no.4, pp.507-515, 2002

An Implicit Finite Element Cavitation Algorithm

Fanghui Shi and Rohit Paranjpe[1]

Abstract: This paper describes an implicit finite element cavitation algorithm. The cavitation problem is formulated using the complementarity form. By using the complementarity formulation, the fluid pressure in the non-cavitation region and the density of the air/fluid mixture in the cavitation region are solved simultaneously. The stream-wise biasing approach is used to produce oscillation-free solution at the fluid film reformation boundary. Implicit scheme is implemented to yield stability for time marching. The algorithm is compared with the established finite volume methods, and the robustness and the correctness of the algorithm is verified.

1 Introduction

Analytical tools to support modern bearing design are getting sophisticated. The cavitation effect is a very important factor that should be taken into account in these analytical tools. Depending on the oil supply situation, the inclusion of the cavitation effect can significantly change the prediction of fluid pressure and density distribution, and thereby some important design parameters, such as minimum film thickness, oil flow and power dissipations.

The investigation of the cavitation effect in lubrication can be dated back to Jakobsson and Floberg (1957) and Olsson (1965). The theory they developed is now known as JFO theory and is based on the conservation of mass. However, a successful numerical algorithm implementing the JFO theory did not appear until the work of Elrod and Adams (1974). In fact, although satisfying the JFO condition, their work is alternative and more based on the physics of the fluid. They artfully used fluid compressibility and developed a universal differential equation governing the fluid behavior in the lubrication region and the fluid/gas mixture behavior in the cavitation region. This basic idea was extended in a later paper by Elrod (1981), in which he introduced the concept of cavitation index (the switching function between lubrication and cavitation regions), and refined the differencing scheme. He used a central differencing scheme for the Couette flow in the full film region and a backward scheme for the flow in the cavitation region. However, the differencing scheme at the lubrication/cavitation boundary did not have a theoretical backing and was developed 'after considerable experimentation'. This subject was studied thoroughly by Vijayaraghavan and Keith (1989, 1990a, b and c). They solved the cavitation problem more rigorously and systematically by using some well-developed CFD techniques, such as higher order artificial viscosity, grid transformation and adaptive meshing etc. Woods and Brewe (1989) successfully used the multigrid method to accelerate the Elrod algorithm (Elrod, 1981). Similar to Elrod's work, Payvar and Salant (1992) introduced their version of this universal differential equation. They dropped the fluid compressibility and made the equation cleaner. The idea is easy for computer programming and yields satisfactory results. In the Elrod scheme and its variants, the fluid pressure and the partial film content is connected by the switching function and the bulk compressibility modulus. Mathematically, the universal differential equation is actually an elliptic equation and a hyperbolic equation linked by the switching function. When the solution is in progress, the characteristics of the equation may change due to the changes in the switching functions. Consequently, the equation becomes nonlinear, because of its solution-dependent coefficients. Shi and Salant (2000) introduced a scheme in which the characteristic of the differential equation stays elliptic during the solution process. The switching function is used not to change the characteristics of the equation but just as a correction pointer on the solution. This method makes the differential equation linear, and thus makes it possible to take advantage of the matrix factorization technique during the iteration process.

All the above-mentioned cavitation algorithms were de-

[1] Methods Development, Synthesis and Analysis Department
General Motors Powertrain
30003 Van Dyke Ave
Warren, MI 48090

veloped using finite volume or finite difference methods, and thus these two numerical methods have become the major choices to analyze lubrication problems involving cavitation effects. Compared with finite volume/finite difference space discretization methods, the finite element method has an inherent advantage in its superior ability to handle complex geometry and boundary conditions, such as stationary and moving holes and grooves on the journals or the bearings for the lubrication problems. The first finite element cavitation algorithm is introduced by Goenka (1984), however the algorithm used Reynolds boundary condition and was not mass-conserving. Due to its robustness and effectiveness to locate the film rupture boundary, Goenka's approach has been used in many finite element lubrication analyses. A finite element cavitation model that conserves mass was later introduced by Kumar and Booker in 1991. The model is capable of predicting the transient evolution of cavitation in fluid film by using an explicit time marching scheme. Apply the same complementarity approach as in Goenka's work, Bonneau et. al. (1995) introduced a conservation flow method to predict cavitation boundaries using the JFO moving conditions. In their work, explicit time marching scheme is also used to determine the location of film reformation. It is well-known that in explicit time marching schemes, relatively small time steps needs to be used for stability and the steady state problem has to be solved through a series of time marching, which affects the computational efficiency.

In this work, an implicit finite element mass-conserving cavitation algorithm is developed. In this algorithm, the fluid pressure in the non-cavitation region and the reduced fluid density in the cavitation region are solved simultaneously using the complementarity relations. The algorithm employs an implicit time marching scheme, which is theoretically stable. It is capable of handling both dynamic and quasi-steady state cavitation problems with satisfactory computational efficiency and is easy for the finite element implementation.

2 Formulations

As described in Shi and Salant (1999), the fluid behavior for cavitation problem is governed by the Reynolds equation for compressible fluids and is constrained by a set of physical conditions. The set of physical constraints are that fluid endures pressure higher than cavitation pressure in the non-cavitation region and the cavitation pressure in the cavitation region, meanwhile, the fluid has negligible compressibility in the non-cavitation region and significant compressibility in the cavitation region. The mathematical equation are simply written as,

$$\nabla \cdot (\frac{h^3}{\eta}\nabla p) = 6\nabla \cdot (\mathbf{u}\rho h) + 12\frac{\partial \rho h}{\partial t} \tag{1}$$

with the constraints,

$$\rho = \rho_{ncav}(x,y) \not\subset \Omega_{cav} \text{ and } \rho < \rho_{ncav}(x,y) \subseteq \Omega_{cav} \tag{2}$$

$$p > p_{cav}(x,y) \not\subset \Omega_{cav} \text{ and } p = p_{cav}(x,y) \subseteq \Omega_{cav} \tag{3}$$

where ρ_{ncav}, the density in the non-cavitation region, and p_{cav}, the pressure in the cavitation region, are known dimensionless constants,

$$\rho_{ncav} = 1 \tag{4}$$

$$p_{cav} = 0 \tag{5}$$

2.1 Couette Flow Approximation

Cavitation computations were shown by Vijayaraghavan and Keith (1989, 1990) to have significant resemblance with transonic flow computations. Thus, an 'artificial viscosity' or 'artificial dissipation' term also needs to be added to the cavitation computations. Such addition is able to yield a central difference for the non-cavitation region and a backward difference for the cavitation region. Using the mass flux biasing approach (Tannehill et. al., 1997), the equivalent mass flux along the streamline can be written as,

$$\mathbf{u}\rho^* h = \mathbf{u}\rho h - (1-C)\Delta \mathbf{s}\frac{\partial u\rho h}{\partial S} \tag{6}$$

where S is the local stream-wise coordinate and ρ^* is the equivalent density to be solved. C is the local cavitation index (1 for full film, 0 for cavitation).

2.2 Squeeze Flow Approximation

The squeeze term in equation (1) is approximated by using the fully implicit scheme, superscript i for the current time step is dropped for brevity,

$$\frac{\partial \rho h}{\partial t} = \frac{\rho h - \rho^{i-1}h^{i-1}}{\Delta t} \tag{7}$$

2.3 Finite Element Formulation

Substituting equation (6) and (7) into equation (1) and applying Galerkin finite element method (assuming both p and ρ as unknowns), we have,

$$\sum_e \int_e N^T \nabla \cdot \left(\frac{h^3}{\eta}\nabla p\right) dA$$
$$= 6\sum_e \int_e N^T \nabla \cdot \left[(\mathbf{u}\rho h) - (1-C)\,\Delta \mathbf{s}\frac{\partial u \rho h}{\partial S}\right]$$
$$+ 2N^T \left(\frac{\rho h - \rho^{i-1}h^{i-1}}{\Delta t}\right) dA \tag{8}$$

where N^T is the shape function vector which depends on the element type chosen. Equation (8) can then be further written in the following form,

$$\left[\sum_e \mathbf{K}_p^e\right]_{N\times N} \{p\}_{N\times 1} = \left[\sum_e \mathbf{K}_p^e\right]_{N\times N} \{\rho\}_{N\times 1} - \left[\sum_e b^e\right]_{N\times 1} \tag{9}$$

Where the element matrices and the vector are of the size of 3×3 and 3×1 respectively, if three node tri-angular element is used,

$$\mathbf{K}_p^e = -\nabla \mathbf{N}^\mathbf{T} \cdot \nabla \mathbf{N} \int_e \frac{h^3}{\eta} dA$$
$$\mathbf{K}_\rho^e = 6\int_e \mathbf{N}^\mathbf{T} \nabla \cdot (\mathbf{u}\mathbf{N}h)\,dA - \mathbf{D} + \frac{12}{\Delta t}\int_e \mathbf{N}^\mathbf{T}\mathbf{N}h\,dA$$
$$\mathbf{b}^e = \frac{12}{\Delta t}\int_e \mathbf{N}^\mathbf{T}\rho^{i-1}h^{i-1}dA \tag{10}$$

The newly developed cavitation matrix D is the contribution of the 'artificial dissipation' term, defined as,

$$\mathbf{D} = 6\nabla \mathbf{N}^T \cdot \begin{bmatrix} \cos^2\theta & \cos\theta\sin\theta \\ \sin\theta\cos\theta & \sin^2\theta \end{bmatrix} \nabla \mathbf{N} \cdot \tag{11}$$
$$\begin{bmatrix} (1-C_i)u_i h_i & 0 & 0 \\ 0 & (1-C_j)u_j h_j & 0 \\ 0 & 0 & (1-C_k)u_k h_k \end{bmatrix} l^e A^e$$

where θ is the angle between Couette flow direction and positive x direction, on which the finite element mesh is based, and the characteristic element length l^e is defined as:

$$l^e = \frac{1}{3}\sqrt{\frac{\left[(l_x^e u_x)^2 + (l_y^e u_y)^2\right]}{u_x^2 + u_y^2}} \tag{12}$$

By using equation (10) and (11), we are able to handle the situations where the Couette flow direction is different from the grid line direction, which are always required to be the same in the existing finite volume cavitation algorithms. The cavitation matrix D is similar to the 'balancing dissipation' term proposed by Kelly et. al. (1980) in order to solve convective diffusion problems using finite element methods.

2.4 Complementarity Relations

The fluid constraint equations (2), (3), (4), (5) pose a complementarity relations on the governing equation (1). In terms of computation, the relations indicate there is one and only one unknown to be solved in any row of the system of equation (9). Depending on the cavitation situation, this unknown could either, on the L.H.S, be the fluid pressure in the non-cavitation region, or on the R.H.S., be the reduced density in the cavitation region. Introducing an universal variable with dual interpretations: pressure in the non-cavitation region (C=1), or the reduced density in the cavitation region (C=0),

$$\Phi = Cp + (1-C)\rho = Cp_{ncav} + (1-C)\rho_{cav} \tag{13}$$

The system of equation (9) can be rearranged, with the assistance of grouping unknown p_{ncav} and ρ_{cav} together into one universal variable Φ, into the following matrix form,

$$\mathbf{A}\Phi = \mathbf{B}C - \mathbf{E} \tag{14}$$

where

$$\mathbf{A} = \left[\sum_e \mathbf{K}_p^e\right]_{N\times N} \mathbf{C}_{N\times N} - \left[\sum_e \mathbf{K}_\rho^e\right]_{N\times N} (\mathbf{I}_{N\times N} - \mathbf{C}_{N\times N})$$
$$\mathbf{B} = \left[\sum_e \mathbf{K}_\rho^e\right]_{N\times N}$$
$$\mathbf{E} = \left[\sum_e b^e\right]_N \tag{15}$$

and the diagonal matrix $\mathbf{C}$ is defined to have the cavitation indices on its diagonal entries.

3 Algorithms

1. At any time transient, results from previous time transient are assumed known. The vector **E** in equation (15) can be obtained by assembling the element vector $\mathbf{b}^e$ in equation (10).

2. During iterations for a given time transient, the cavitation index matrix **C** is known, (assumed full film everywhere for the 1st iteration, except for the locations where density boundary conditions are applied). The global matrices $\mathbf{K}_p$ and $\mathbf{K}_\rho$ can be obtained by assembling the element matrices K_p^e and K_ρ^e provided in equation (10), and the cavitation matrix **D** given in equation (11).

3. Evaluate matrices **A** in equation (15). Computationally, the j^{th} column of A is occupied by the j^{th} column of $\mathbf{K}_p$ (if C_j=1) or the jth column of -$\mathbf{K}_\rho$ (if C_j=0).

4. Solve for universal vector Φ by using equation (14).

5. Check fluid constraints for all nodes. a. If C_j=1 and $\Phi_j < P_{cav}$then C_j=0; b. If C_j=0 and $\Phi_j > \rho_{ncav}$then C_j=1.

6. Iterate from step 2 until the cavitation index matrix **C** converges (no jump of C between 0 and 1 is detected)

7. Calculate P_{ncav} and ρ_{cav} from the converged universal variable Φ and cavitation index by using equation (13).

It should be pointed out that the order of accuracy of the proposed FEM algorithm depends on the order of the element chosen to discretize the problem. For instance, linear element can provide 2nd order accuracy for hydrodynamic pressure in the full film region and 1st order accuracy for the reduced density in the cavitation region. Higher orders of accuracy for hydrodynamic pressure can be achieved by using non-linear elements. However, the improvement of the accuracy for the reduced density in the cavitation region by using non-linear element is very limited since linear element is already sufficient to approximate the constant Couette flow. Such FEM algorithm has been embedded into the Newton-Raphson scheme and has been implemented in the General Motors internal code FLARE (Goenka, et. al., 1992). The simultaneous solution of the unknown hydrodynamic pressure, the reduced density, the elastic deformation, and the secondary motions in the bearing is found very robust and efficient. Detailed description of such scheme goes beyond this paper and will be given in a future paper.

4 Results

A series of computations are performed based on a domain that has the size of 1×0.25(length by width or $x \times y$) and a sample film thickness distribution, $h(x,y) = 1.1 + \cos(2\pi x)$. The viscosity η of the fluid is assumed to be 1 and the sliding speed **u** is assumed to be 83.33**i** along the x direction. Cyclic boundary conditions are imposed in the x direction and fixed pressure boundary conditions (p=1) are imposed in the y direction. The finite element mesh used in the computations is of size 65×65 with equal spacing.

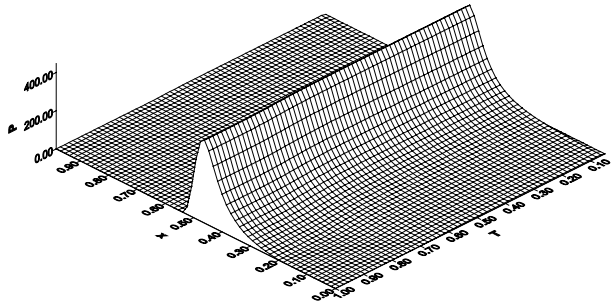

Figure 1 : History of hydrodynamic pressure along centerline (y=0.5)

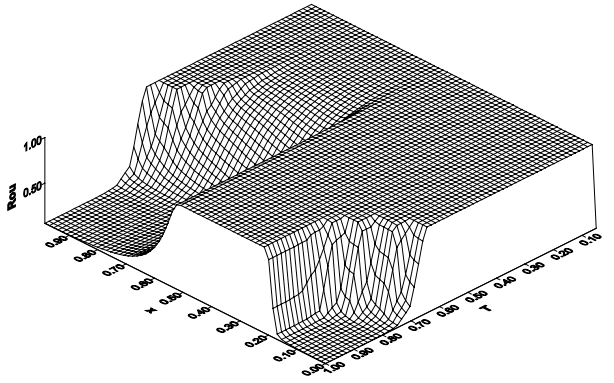

Figure 2 : Dynamic evolution of cavitation at centerline (y=0.5)

The fluid is initially complete and cavitation is allowed to develop. The history of the hydrodynamic pressure

at the centerline (y=0.5) is plotted for each time transient in Figure 1. Note that logrithmatic time scale, $T = \frac{\log_2(time \times 10^6)}{20}$, is used here to reveal the detailed history. The peak hydrodynamic pressure is found dropped, due to the development of the cavitation region, from 458.956 at T=0.05 to 446.614 at T=1.0 (the drop may not be detectable from the graph). The dynamic evolution of cavitation region is shown in Figure 2. The graph clearly shows the development of cavitation region and the steady state is found to have been reached when $T > 0.9$. Other noticed aspect is that density discontinuity at the fluid film reformation boundary becomes severe only when approaching the steady state. The steady state cavitation is also obtained by marching with a large time step. The results are the same as the one obtained previously by marching with a series of small time steps. The reduced density and the hydrodynamic pressure along the centerline using the current FEM are compared against the one obtained using some established FVM (Finite Volume Method). These methods include the Elrod method (Elrod, 1981), the second order upwind method (Vijayaraghavan and Keith, 1990) and the shifted upwind method (Payvar and Salant, 1992). The results of comparison, as shown in Figure 3, are satisfactory. The 2D pressure and density distributions calculated using current FEM and using Elrod's FVM are shown in Figure 4-Figure 7. It is shown in Figure 4 and Figure 5 that the pressure distributions are almost identical. However, some differences at the film reformation boundaries can be found in density distribution plots Figure 6 and Figure 7. The reason is that while the artificial dissipation term, described earlier in equation (11), removes the oscillation in the direction of Couette flow, the existence of the FEM stencil in the cross direction causes the density variations. Thus, it is observed that the density vari-

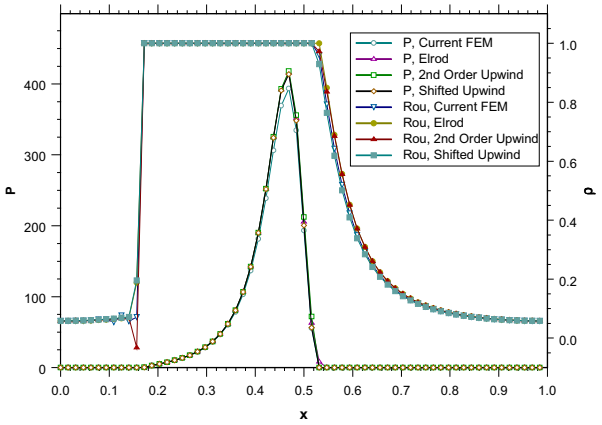

Figure 3 : Accuracy comparision against some established FVM algorithms

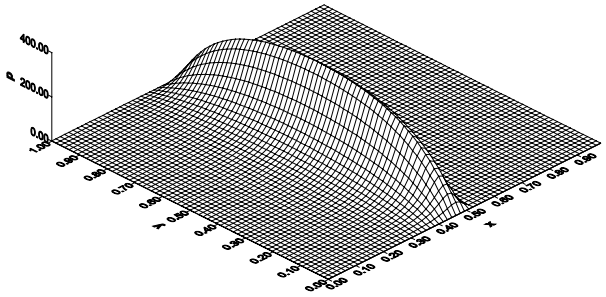

Figure 4 : Pressure distribution obtained using current FEM

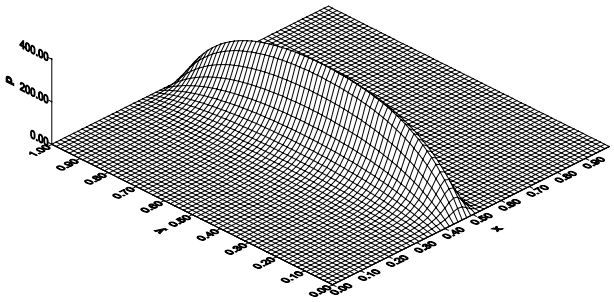

Figure 5 : Pressure distribution obtained using Elrod's FVM

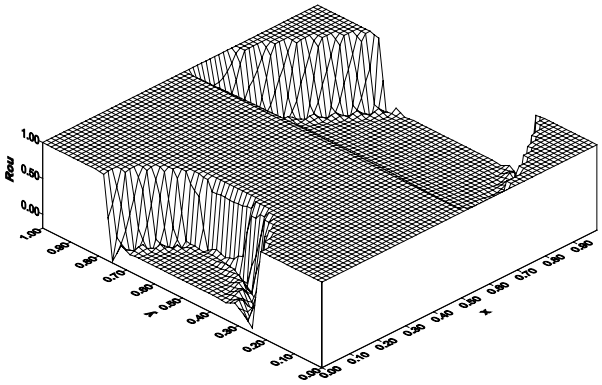

Figure 6 : Density distribution obtained using current FEM

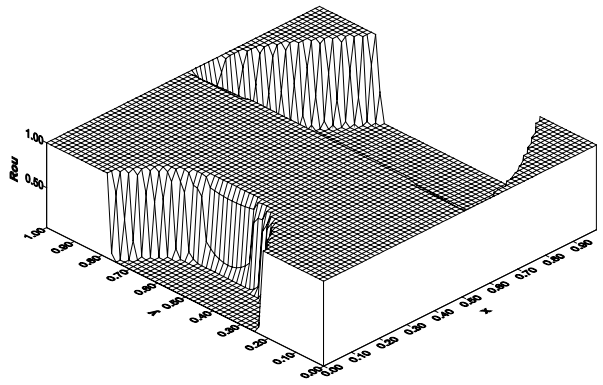

Figure 7 : Density distribution obtained using Elrod's FVM

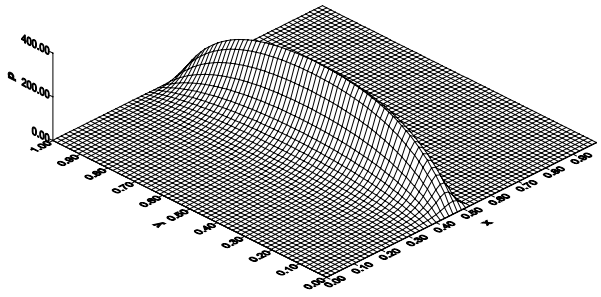

Figure 8 : Presure distribution with both x and y velocity components

ations are relatively noticeable at the nodes whose cross directional neighboring node is on the film reformation boundary where the density discontinuity takes place, as shown in Figure 6. Nevertheless, it should be pointed out that such variations are very local and do not violate the conservation of mass. FVMs use a 1D stencil (if the Couette flow direction and the grid line direction is the same) to approximate the Couette flow and does not have this problem, therefore a smooth density distribution can be obtained, as shown in Figure 7.

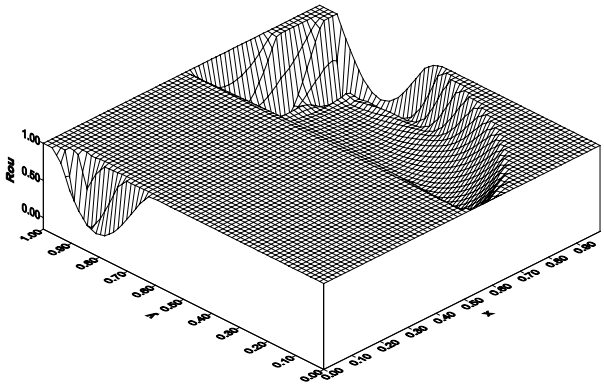

Figure 9 : Density distribution with both x and y velocity components

Although the 2D FEM stencil used to approximate Couette flow causes density variations in the cross direction, it is capable of handling arbitrary meshes, and does not require the Couette flow direction the same as the grid line direction. To verify this judgement, a new test case is used with width (y) direction component of sliding speed **u** added. The sliding speed for the new case is assumed to be 83.33i+41.67j with all the remaining conditions the same. The pressure and density distributions are shown in Figure 8 and Figure 9. The cavitation region is found reduced because of the additional Couette flow in the width direction.

A lubrication analysis is performed for a typical connecting-rod bearing, shown in Figure 10. The bearing configuration is symmetric about the axial direction and carries a 75×6 mesh with equal spacing in the circumferential and axial direction respectively. The configurations and operating conditions of the engine bearing are given as follows: bearing radius 24.529mm, bearing length 20.196mm, bearing clearance 0.0254mm, bearing eccentricity 0.025mm, size of the hole on the journal 6mm, circumferential location of the hole 60deg, oil feed

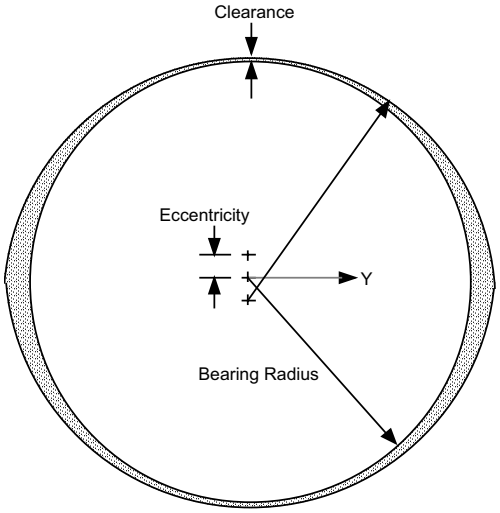

Figure 10 : Typical connecting-rod bearing in automotive engine

pressure 3×10^5pa, oil viscosity 0.00852pa.s, and engine speed 2031rev/s. The bearing loads (Fx, Fy) as functions of crank angle are given in Figure 11, assuming x is the direction along the connecting rod from the bearing to the pin.

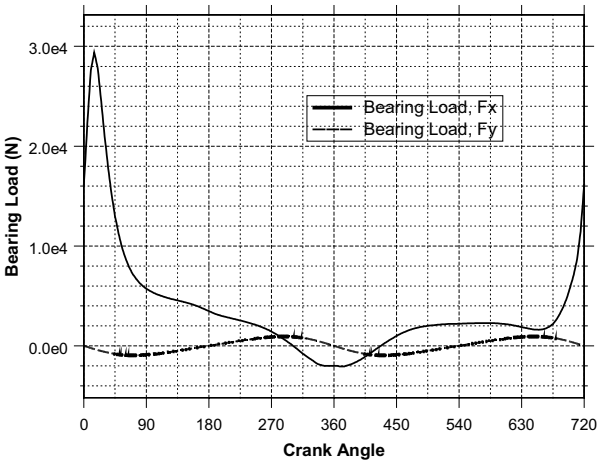

Figure 11 : Bearing loads used in the calculations

One important effect of the mass conserving cavitation is shown in the Figure 12, which displays the journal orbits predicted with and without mass conserving cavitation. It can be detected that the ignorance of the cavitation effect can lead to a prediction of smaller journal orbit. To further validate the FEM algorithm, the results are compared, in the following, with the one obtained by using the combination of Elrod's FVM and Newton-Raphson (NR) scheme, as described in (Paranjpe and Goenka, 1990). For brevity, these two methods (current FEM+NR and Elrod's FVM+NR) are referred to as FEM and FVM respectively. The simulation takes about 7 minutes on a HP5000 workstation to achieve convergence (periodicity). The minimum bearing oil film thickness (MBOFT) for each crank angle, as shown in Figure 13, agrees well between the two methods. The minimums of MBOFT, both occurred at around 40 degree, however, are noticed to have 10% difference (0.720 μm for FEM vs. 0.827 μm for FVM). The maximum hydrodynamic pressures (MHP) are shown in Figure 14. The comparison is satisfactory with a maximum error of 3% (258.9 Mpa for FEM vs. 266.9 Mpa for FVM), occurred at the location where the maximum of MHP takes place. Figure 15 shows the power loss curves with an average of 0.535 kw for FEM and 0.557 kw for FVM, equaling to 4% difference. The bearing flows (in flow and out flow) are

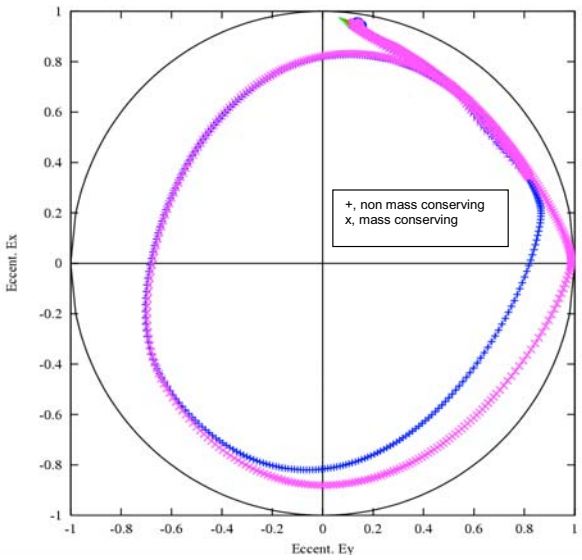

Figure 12 : Journal orbits predicted with and without Mass Conserving Cavitation, eccentricity Ey is squeezed by a factor of 1.6 to account for the eccentric bearing effect.

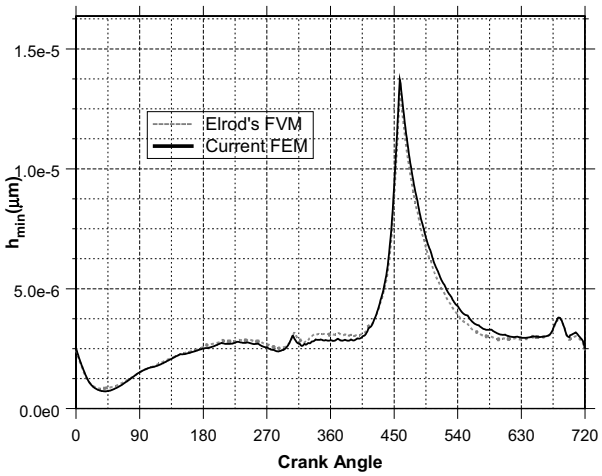

Figure 13 : Calculations of minimum film thickness using Elrod's FVM and current FEM.

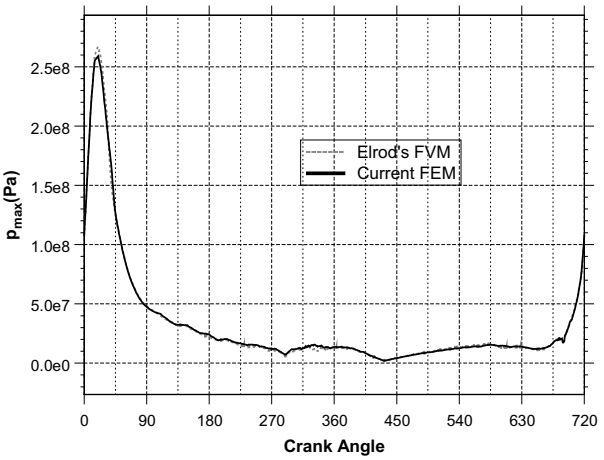

Figure 14 : Calculations of the maximum pressure using Elrod's FVM and current FEM.

found balanced in a period an engine cycle using both methods. Out flow results (average of 1.777×10^{-6} m^3/s for FEM and 1.798×10^{-6} m^3/s for FVM) are plotted in Figure 16 and are found almost identical. In addition to the differences between FEM and FVM in discretizing the Reynolds' equation, different time marching schemes for the secondary motion (implicit in current work and explicit in Paranjpe and Goenka, 1990) are believed to cause the results to be slightly different.

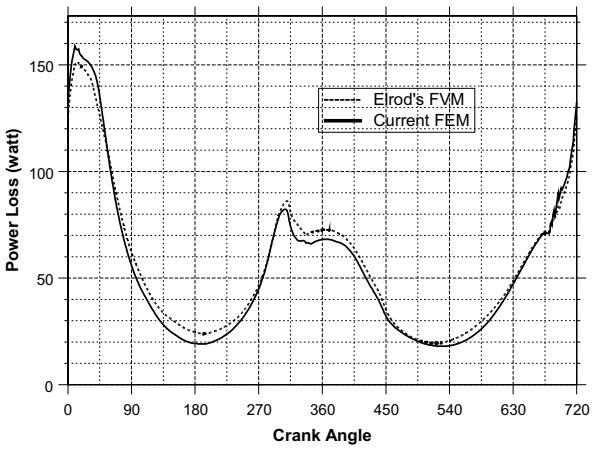

Figure 15 : Calculations of the power loss using Elrod's FVM and Current FEM.

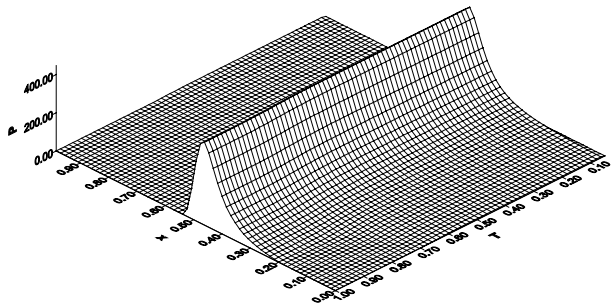

Figure 16 : Computations of the bearing flow using Elrod's FVM and current FEM.

5 Conclusions

A FEM-based implicit cavitation algorithm is developed. The hydrodynamic pressure in the non-cavitation region and the reduced density in the cavitation region are solved simultaneously. The stream-wise biasing approach is used to produce oscillation-free solution at the fluid film reformation boundary. Implicit scheme is implemented to yield stability for time marching. The algorithm is tested against the established finite volume methods, the robustness and the correctness of the algorithm is verified.

References

Bonneau, D., Guines, D., Frene, J. and Toplosky, J. (1995): EHD Analysis, Including Structural Inertia Effects and a Mass-Conserving Cavitation Model, *ASME Journal of Tribology*, Vol. 117, pp. 540-547.

Elrod, H. G., and Adams, M. L. (1974): A Computer Program for Cavitation and Starvation Problems, *Cavitation and Related Phenomena in Lubrication*, Mechanical Engineering Publication, New York, NY, pp. 37-41.

Elrod, H. G. (1981): A Cavitation Algorithm, *ASME Journal of Tribology*, Vol.103, pp. 350-354.

Goenka, P. K. (1984): Dynamically Loaded Journal Bearings: Finite Element Method Analysis, *ASME Journal of Tribology*, Vol.106, pp. 429-439.

Goenka, P. K., and Paranjpe, R. S. (1992): A Review of Engine Bearing Analysis Methods at General Motors, *SAE* Technical Paper No. 920489

Jakobsson, B., and Floberg, L. (1957): The Finite Journal Bearing Considering Vaporization, *Transactions of Chalmers University of Technology*, Guthenberg, Swe-

den, 190.

Kelly, D. W., Nakazawa, S., and Zienkiewicz O. C. (1980): A Note on Upwinding and Anisotropic Balancing Dissipation in Finite Element Approximations to Convective diffusion Problems, *International Journal for Numerical Methods in Engineering*, Vol. 15, pp. 1705-1711.

Kumar, A., and Booker, J. F. (1991a): A Finite Element Cavitation Algorithm, *ASME Journal of Tribology*, Vol. 113, pp. 276-286.

Olsson, K. O. (1965): Cavitation in Dynamically Loaded Bearing, *Transactions of Chalmers University of Technology*, Guthenberg, Sweden, 308.

Paranjpe, R. S. and Goenka, P. K. (1990): Analysis of Crankshaft Bearings Using a Mass Conserving Algorithm, STLE Tribology Transactions, Vol. 33, pp. 333-344.

Payvar, P. and Salant, R. F. (1992): A Computational Method for Cavitation in a Wavy Mechanical Seal, *ASME Journal of Tribology*, Vol. 114, pp. 199-204.

Shi, F. and Salant, R. F. (1999): A Soft Mixed-Elastohydrodynamic Lubrication Model with Interasperity Cavitation and Surface Shear Deformation, *ASME Journal of Tribology*, Vol. 122, pp. 308-316.

Tannehill J. C., Anderson, D. A., and Pletcher R. H. *Computational Fluid Mechanics and Heat Transfer*, Taylor and Francis Pres, 1997.

Vijayaraghavan, D., and Keith, Jr., T. G. (1989) Development and Evaluation of a Cavitation Algorithm, *STLE Tribology Transactions*, Vol. 32, No. 2, pp. 225-233.

Vijayaraghavan, D., and Keith, Jr., T. G. (1990a): An Efficient, Robust and Time Accurate Numerical Procedure Applied to a Cavitation Algorithm, *ASME Journal of Tribology*, Vol. 112, No. 1, pp. 44-51.

Vijayaraghavan, D., and Keith, Jr., T. G. (1990b): Grid Transformation and Adaption Techniques Applied in the Analysis of Cavitated Journal Bearings, *ASME Journal of Tribology*, Vol. 112, No. 1, pp. 52-59.

Vijayaraghavan, D., and Keith, Jr., T. G. (1990c): Analysis of a Finite Grooved Misaligned Journal Bearing Considering Cavitation and Starvation Effects, *ASME Journal of Tribology*, Vol. 112, No. 1, pp. 60-67.

Woods, C. M. and Brewe, D. E. (1989): The Solution of the Elrod Algorithm for a Dynamically Loaded Journal Bearing using Multigrid Techniques, *ASME Journal of Tribology*, Vol. 111, pp. 302-308.